

Fast Segmentation of Sub-Cellular Organelles

Dilip K. Prasad

*School of Computer Engineering
Nanyang Technological University
Singapore, 639798*

dilipprasad@gmail.com

Chai Quek

*School of Computer Engineering
Nanyang Technological University
Singapore, 639798*

ashcquek@ntu.edu.sg

Maylor K. H. Leung

*Faculty of Information and Communication Technology
Universiti Tunku Abdul Rahman(Kampar)
Malaysia*

asmkleung@gmail.com

Abstract

Segmentation and counting sub-cellular structure of size range $0.1\mu\text{m}$ to $1\mu\text{m}$ is a very challenging problem even for medical experts. Image acquisition time for the state-of-the-art fluorescence microscopes is about 1-5 seconds. A fast and efficient method for segmentation and counting of sub-cellular structure is proposed for concurrent post-processing of fluorescence microscopy images. The proposed method uses a hybrid combination of several image processing techniques and is effective in segmenting the sub-cellular structures in a fast and effective manner.

Keywords: Segmentation, Bio-cell Organelles, Fluorescence Microscopy, Ellipse Detection.

1. INTRODUCTION

Cell and sub-cellular segmentation in biomedical images is helpful in diagnosis and cell biology research. Often manual segmentation and classification is slow since one image may contain numerous cells or sub-cellular structures. Automatic segmentation software can be used for this purpose but the accuracy is often low and is often unable to filter away the artifacts on its own.

Here, a segmentation algorithm for cells or sub-cellular structures that can be modeled as elliptic shapes is proposed. Examples of such datasets can be found in [1-4]. The dataset considered in this paper is a dataset of images of mixed cell organelle types (mitochondria and lysosomes) [4]. Fluorescence confocal microscope is used to generate the images. Preprocessing of the images leads to cleaner images in which the cells appear in the foreground (for example as shown in FIGURE 3(a)). These images are used as input images for the proposed algorithm. It is highlighted that in several of the images, no sub-cellular structures are seen. Thus, images that contain sub-cellular features are selected manually. There are a total of 444 such images, each of size 1349×1030 pixels.

The proposed algorithm employs three simple blocks and the core of the algorithm is a least squares ellipse fitting method. The algorithm is tested on a dataset of images of two types of sub-cellular structures [4] and the algorithm shows a good performance. Further it is quite fast and easily parallelizable. Thus, with some code optimization, it can be made real time.

The proposed algorithm is presented in section 2. The dataset for testing the proposed algorithm and the control parameters chosen for this dataset are also discussed in section 2. The results are presented in section 3. The paper is concluded in section 4.

2. PROPOSED ALGORITHM

The proposed algorithm employs three simple blocks, viz., pre-processing, ellipse fitting, and ellipse selection. The flowchart of the proposed algorithm is shown in FIGURE 1.

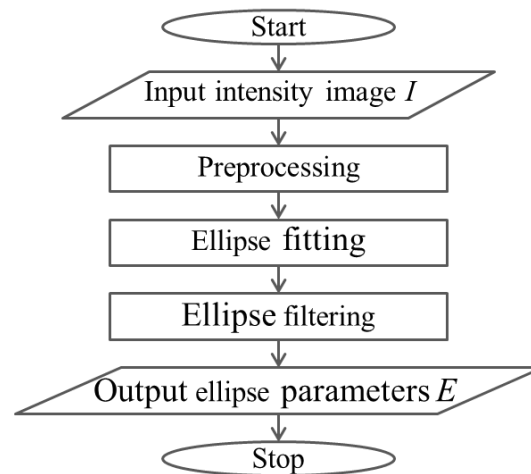


FIGURE 1: Flowchart of the proposed method.

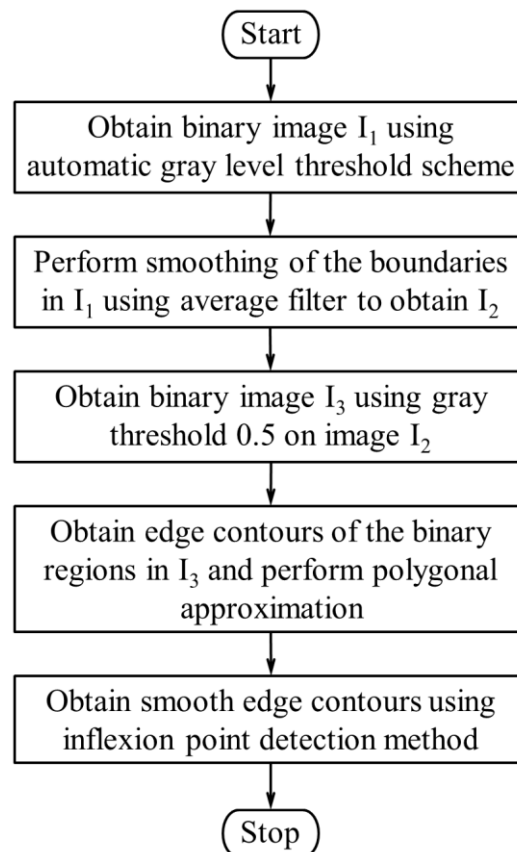


FIGURE 2: Flowchart for preprocessing block.

2.1 Preprocessing Block

It is assumed that the input is the intensity image I (gray scale 0-255). The flowchart of this block is presented in FIGURE 2. One of the critical aspects is the choice of the threshold level for obtaining the binary images. The images in the biomedical dataset obtained using microscopy can suffer from several issues. Examples include low contrast, bleaching (background illumination), noise, scattering from irrelevant organelles, etc. However, assuming that the same instrument and measurement setup is used to generate the images in a particular dataset, a suitable threshold level t_1 can be determined *a priori* for binarizing the image (step 1 in FIGURE 2), where the binary image is being referred to as I_1 .

In order to deal with extremely low contrast features, it is preferable to use a low value of t_1 . Consider for example the image in FIGURE 3(a). The highlighted circle shows a region that contains a cell but is invisible due to extremely low contrast. As a consequence, this cell is present in the binarized image when $t_1 = 5$ is used (FIGURE 3(b)) but absent when $t_1 = 15$ is used (FIGURE 3(c)). It is also notable that artifacts due to noise appear when low threshold is used.

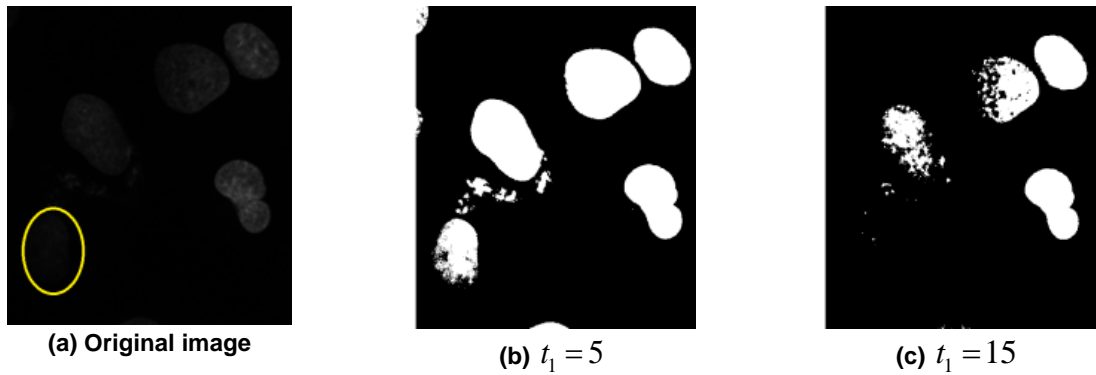


FIGURE 3: Example of the effect of threshold value t_1 on the binary image I_1 .

Thus, a suitable selection of the threshold is quite important. A statistical scheme is proposed here for choosing the value of threshold t_1 . For determining the suitable value of t_1 , the histogram of each image in the dataset is generated for gray levels 0 – 255. Let the histogram count for a gray level $g \in \{0, 255\}$ for an image I be denoted as $h(g, I)$. Cumulative histogram is generated for each gray level and image is computed as:

$$\bar{C}(g, I) = \sum_{g'=0}^g h(g', I) \quad (1)$$

Then, the normalized cumulative histogram is computed as follows:

$$C(g, I) = \frac{\bar{C}(g, I)}{\max(\bar{C}(g, I) | \forall g)} \quad (2)$$

The values of the normalized cumulative histogram for a given gray level g are averaged for all the images and plotted in FIGURE 4(a). It is seen that the images have low intensity since only lower gray levels (till $g = 100$) have contribution in the images. A zoom-in of FIGURE 4(a) is provided in FIGURE 4 (b) where only $g = 0$ to 31 is considered). It is seen that $g = 4$ is sufficient for more than 80% of the cumulative histogram of the images. Thus, $t_1 = 4$ is chosen as the threshold for binarizing the images (step 1 of FIGURE 2).

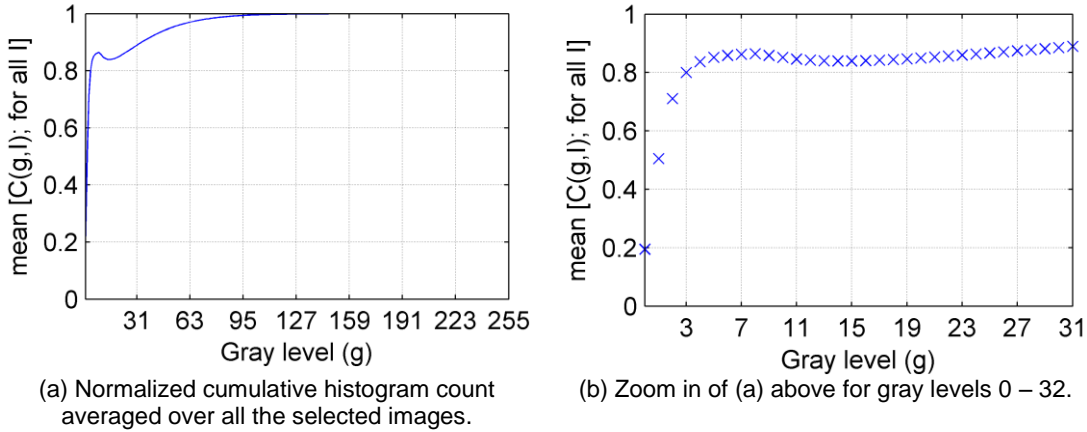


FIGURE 4: Normalized cumulative histogram averaged over all the images used for choosing the value of threshold t_1 .

Yet, as shown in FIGURE 3, the boundaries of the cells may not be well defined due the binarization. Thus, a spatial mean filter of size 5 is applied on the binary image I_1 to get a gray scale image I_2 with smoother features (step 2 in FIGURE 2). The image I_2 is binarized again using a threshold value of 0.5, since the image I_2 obtained after applying average filter on the binary image I_1 (step 3 in FIGURE 2) is a gray scale image. The final binary image used for further processing is denoted as I_3 .

The edge contours of the white regions in I_3 are extracted (step 4 in FIGURE 2) and are denoted by index $e=1$ to \hat{e} . For each edge e , polygonal approximation of the edge is derived using RDP-mod proposed in [5] (step 4 in FIGURE 2). Other polygonal approximation approaches may be considered as well [5-15]. The polygonal approximation of the edge contour is consequently used to remove the inflexion points and obtain smooth edges $e'=1$ to \hat{e}' using the algorithm for removing inflexion points appearing in section 2 of [16] (step 5 in FIGURE 2), see also [17-19].

2.2 Ellipse Fitting Block

This block calls a least squares based ellipse fitting method for each edge $e'=1$ to \hat{e}' . If the method generates a valid ellipse, the geometric parameters of the ellipse (length of semi-major axis a , length of semi-minor axis b , x-coordinate of the center x_0 , y-coordinate of the center y_0 , and the angle made by semi-major axis with the x -axis α of the fitted ellipse) is appended in the array containing the parameters of ellipses E .

The choice of the ellipse fitting method has a significant impact on the overall performance of the method. Hough transform based methods have several problems like a huge number of samples are required to obtain robust results, five-dimensional parameter space of ellipses is difficult to deal with computationally, and the whole process can be significantly time consuming. Hybrid methods for high end applications [16, 20, 21], which generally give high accuracy, are slow and computationally expensive. They also include other very sensitive steps like tangent estimation [22-27]. So, least squares based methods for fitting ellipses can be used. In our numerical results, it shall be shown that the geometry based least squares fitting method presented in [28] performs better than other least squares methods.

For the sake of completeness, the algorithmic structure of the geometry based least squares fitting method presented in [28] is reproduced here. For a sequence of pixels $\{P_i(x'_i, y'_i); i=1$ to $N\}$, we intend to find the parameters a, b, θ_c, x_c , and y_c , such that the residue

given in eqn. (3) is minimized. Here, $|\cdot|$ denotes the absolute value in the case of scalars and Euclidean norm in the case of vectors.

$$r'_i = |y'_i - m'_i x'_i - c'_i|. \quad (3)$$

Step 1: Compute $\tilde{x}_i = x'_i - \tilde{x}$, $\tilde{y}_i = y'_i - \tilde{y}$ where (\tilde{x}, \tilde{y}) are given by eqn. (4).

$$\tilde{x} = \frac{1}{N} \sum_{\forall i} x'_i; \quad \tilde{y} = \frac{1}{N} \sum_{\forall i} y'_i \quad (4)$$

Step 2: Form the matrix \mathbf{X} and the vector \bar{Y} as given in eqns. (5) and (6).

$$\mathbf{X} = \begin{bmatrix} \vdots & \vdots & \vdots & \vdots & \vdots \\ -\tilde{x}_i^2 & -\tilde{x}_i \tilde{y}_i & \tilde{x}_i & \tilde{y}_i & -1 \\ \vdots & \vdots & \vdots & \vdots & \vdots \end{bmatrix} \quad (5)$$

$$\bar{Y} = [\tilde{y}_1^2 \quad \tilde{y}_2^2 \quad \dots \quad \tilde{y}_N^2]^T, \quad \bar{Y} \in \mathbb{Z}^N \quad (6)$$

Step 3: Compute $\bar{\Phi}$ using eqn. (7).

$$\bar{\Phi} = (\mathbf{X}^T \cdot \mathbf{X})^{-1} \cdot \mathbf{X}^T \cdot \bar{Y} \quad (7)$$

Step 4: Compute $a, b, \theta_c, \tilde{x}_c$, and \tilde{y}_c using eqns. (8) – (12).

$$a = 2 \frac{\sqrt{\phi_2 \phi_3 \phi_4 - \phi_4^2 \phi_1 - \phi_3^2 - \phi_5 (\phi_2^2 - 4\phi_1)}}{\sqrt{(\phi_2^2 - 4\phi_1) \left((1 + \phi_1) - \sqrt{(1 - \phi_1)^2 + \phi_2^2} \right)}} \quad (8)$$

$$b = 2 \frac{\sqrt{\phi_2 \phi_3 \phi_4 - \phi_4^2 \phi_1 - \phi_3^2 - \phi_5 (\phi_2^2 - 4\phi_1)}}{\sqrt{(\phi_2^2 - 4\phi_1) \left((1 + \phi_1) + \sqrt{(1 - \phi_1)^2 + \phi_2^2} \right)}} \quad (9)$$

$$\theta_c = -0.5 \tan^{-1}(-\phi_2 / (1 - \phi_1)) \quad (10)$$

$$\tilde{x}_c = (\phi_2 \phi_4 - 2\phi_3) / (\phi_2^2 - 4\phi_1) \quad (11)$$

$$\tilde{y}_c = (\phi_2 \phi_3 - 2\phi_1 \phi_4) / (\phi_2^2 - 4\phi_1) \quad (12)$$

Step 5: Compute $x_c = \tilde{x}_c + \tilde{x}$ and $y_c = \tilde{y}_c + \tilde{y}$.

2.3 Ellipse Filtering Block

After fitting ellipses on each edge contour, available *a priori* information about the dataset can be used to filter/remove some unreasonable ellipses. The filtering criteria depend upon the dataset and *a priori* information known about it. For example the imaging resolution and the CCD grid size can be used to determine the size range of the cells and thus the bounds on the lengths of semi-major axis a and semi-minor axis b may be generated. Also, the biological information about the cells can be used to generate an estimate of the maximum ratio of the semi-major and semi-minor axes a/b . In the proposed algorithm, the following filtering criteria have been used:

$$a/b \leq t_2 \quad (13)$$

$$t_3 \leq b \leq t_4 \tag{14}$$

where t_2 , t_3 , and t_4 are the thresholds determined based on the apriori knowledge of the cells and the imaging system. The ellipses satisfying eqns. (13) and (14) are retained. It is known that the size of the lysosomes and mitochondria varies in the range $0.1 \mu\text{m}$ to $1 \mu\text{m}$. Thus, the value of the threshold t_2 is chosen as the ratio of the maximum to the minimum size of these sub-cellular structures, i.e., $t_2 = 10$. Further, based on the general size of the sub-cellular structures in the dataset, the threshold values of t_3 and t_4 are chosen as 10 and 100 respectively.

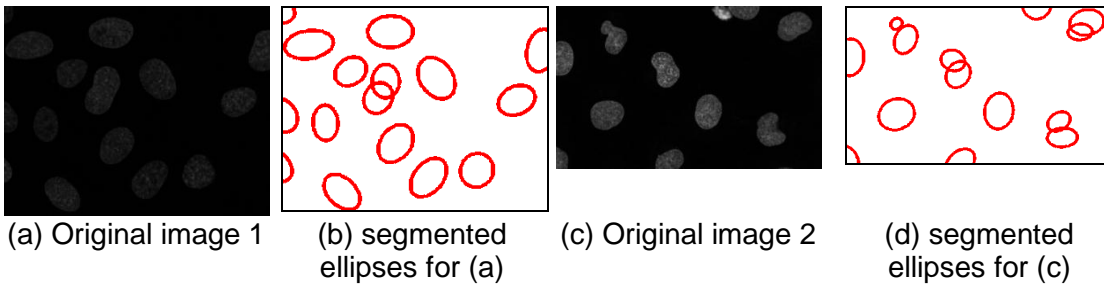


FIGURE 5: Examples of images and ellipses segmented by the proposed method.

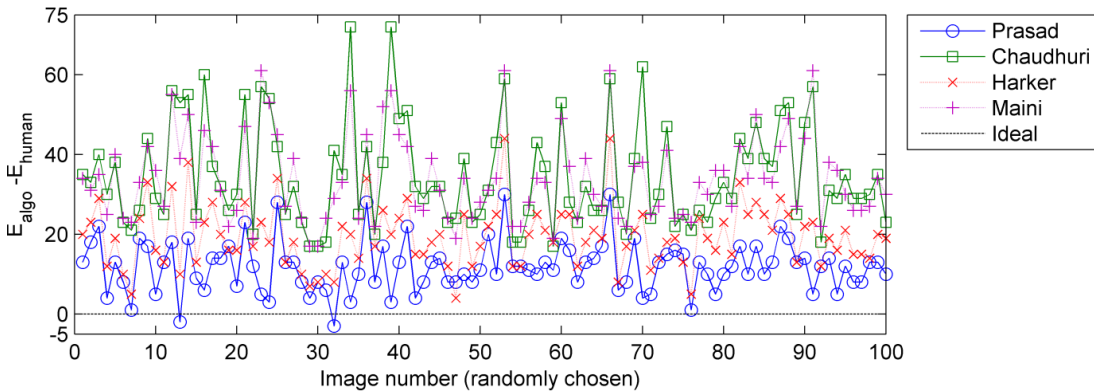


FIGURE 6: Comparison of the performance for various least squares methods. Prasad here represents the unconstrained least squares method presented in section 2.2.

3. NUMERICAL RESULTS

Two examples of the result of the proposed algorithm are shown in FIGURE 5. It is clearly seen that the proposed algorithm can segment the sub-cellular structures very well for low contrast as well as high contrast images, even when some of the sub-cellular structures may be occluded by other structures. The number of ellipses found using the proposed algorithm is denoted using E_{algo} and the number of ellipses found by a human (occluded or otherwise) is denoted by E_{human} . The quantity $E_{\text{algo}} - E_{\text{human}}$ is plotted for 100 randomly chosen images (since it is difficult to collectively present and compare the results for all 444 images) in FIGURE 6. As highlighted in section 2.2, the method chosen for least squares ellipse fitting has a significant impact on the performance of the algorithm. Thus, four methods (Prasad [28] – used in the proposed algorithm and presented in section 2.2, Chaudhuri [29], Harker [30], and Maini [31]) are considered and their performances are compared in FIGURE 6. It is seen that Prasad gives the best performance, thus proving to be the best choice among the four least squares ellipse fitting methods.

	Average time (s)	Standard Deviation
Preprocessing	0.52	0.43
Ellipse fitting (Prasad)	7.86	2.04
Ellipse fitting (Chaudhuri)	9.42	2.93
Ellipse fitting (Harker)	11.27	3.38
Ellipse fitting (Maini)	9.46	3.01
Ellipse filtering	0.02	0.02

TABLE 1: Statistics of computation time without parallel processing

	Average time (s)	Standard Deviation
Preprocessing	0.52	0.43
Ellipse fitting (Prasad)	0.99	0.30
Ellipse fitting (Chaudhuri)	1.21	0.38
Ellipse fitting (Harker)	1.42	0.43
Ellipse fitting (Maini)	1.23	0.39
Ellipse filtering	0.02	0.02

TABLE 2: Statistics of computation time with parallel processing
(parallelization of step 2 of
FIGURE 2 is performed using 8 parallel cores)

The time comparison of the four methods is presented in TABLE 1 (without any parallelization). It is seen that among the four least squares ellipse fitting methods, Prasad takes the least computation time as well. It is also noted that the preprocessing and ellipse filtering steps take very little time. In fact, the computation time for each image can be easily reduced below 1 second by parallelizing the ellipse fitting block. This is illustrated in TABLE 2, where it is shown that the proposed method with Prasad's unconstrained least squares method takes less than 1 second for the most time consuming portion when 8 cores are used. The time performance can be further improved by increasing the number of cores and more effective programming. Thus, the proposed algorithm is capable of providing computation time less than the image acquisition time of a typical fluorescence microscope.

4. CONCLUSION

A fast algorithm is proposed to segment the sub-cellular structures in a dataset of fluorescence microscopy images. The three blocks in the proposed algorithm are simple, fast and effective. The core of the algorithm is the least squares fitting method used in the ellipse fitting block. It is shown that [28] is superior choice than three other least squares fitting methods.

REFERENCES

- [1] S. Kumar, S. H. Ong, S. Ranganath, and F. T. Chew, "Invariant texture classification for biomedical cell specimens via non-linear polar map filtering," *Computer Vision and Image Understanding*, vol. 114, pp. 44-53, Jan 2010.
- [2] G. Dong, N. Ray, and S. T. Acton, "Intravital leukocyte detection using the gradient inverse coefficient of variation," *IEEE Transactions on Medical Imaging*, vol. 24, pp. 910-924, 2005.
- [3] X. Z. Bai, C. M. Sun, and F. G. Zhou, "Splitting touching cells based on concave points and ellipse fitting," *Pattern Recognition*, vol. 42, pp. 2434-2446, Nov 2009.
- [4] T. Peng, G. M. C. Bonamy, E. Glory-Afshar, D. R. Rines, S. K. Chanda, and R. F. Murphy, "Determining the distribution of probes between different subcellular locations through

automated unmixing of subcellular patterns," *Proceedings of the National Academy of Sciences of the USA*, vol. 107, pp. 2944-2949, Feb 2010.

- [5] D. K. Prasad, M. K. H. Leung, C. Quek, and S.-Y. Cho, "A novel framework for making dominant point detection methods non-parametric," *Image and Vision Computing*, 2012.
- [6] D. K. Prasad and M. K. H. Leung, "Reliability/Precision Uncertainty in Shape Fitting Problems," in *IEEE International Conference on Image Processing*, Hong Kong, 2010, pp. 4277-4280.
- [7] D. K. Prasad and M. K. H. Leung, "Polygonal representation of digital curves," in *Digital Image Processing*, S. G. Stanciu, Ed., ed: InTech, 2012, pp. 71-90.
- [8] D. K. Prasad, C. Quek, and M. K. Leung, "A non-heuristic dominant point detection based on suppression of break points," in *Image Analysis and Recognition*. vol. 7324, A. Campilho and M. Kamel, Eds., ed Aveiro, Portugal: Springer Berlin Heidelberg, 2012, pp. 269-276.
- [9] D. K. Prasad, C. Quek, M. K. H. Leung, and S. Y. Cho, "A parameter independent line fitting method," in *Asian Conference on Pattern Recognition (ACPR)*, Beijing, China, 2011, pp. 441-445.
- [10] D. K. Prasad, "Assessing error bound for dominant point detection," *International Journal of Image Processing*, vol. 6, 2012.
- [11] N. Barnes, G. Loy, and D. Shaw, "The regular polygon detector," *Pattern Recognition*, vol. 43, pp. 592-602, 2010.
- [12] A. Carmona-Poyato, R. Medina-Carnicer, F. J. Madrid-Cuevas, R. Muñoz-Salinas, and N. L. Fernández-García, "A new measurement for assessing polygonal approximation of curves," *Pattern Recognition*, vol. 44, pp. 45-54, 2011.
- [13] P. C. Chung, C. T. Tsai, E. L. Chen, and Y. N. Sun, "Polygonal approximation using a competitive Hopfield neural network," *Pattern Recognition*, vol. 27, pp. 1505-1512, 1994.
- [14] T. M. Cronin, "A boundary concavity code to support dominant point detection," *Pattern Recognition Letters*, vol. 20, pp. 617-634, 1999.
- [15] F. Feschet, "Canonical representations of discrete curves," *Pattern Analysis and Applications*, vol. 8, pp. 84-94, 2005.
- [16] D. K. Prasad, M. K. H. Leung, and S. Y. Cho, "Edge curvature and convexity based ellipse detection method," *Pattern Recognition*, vol. 45, pp. 3204-3221, 2012.
- [17] D. K. Prasad and M. K. H. Leung, "An ellipse detection method for real images," in *25th International Conference of Image and Vision Computing New Zealand (IVCNZ 2010)*, Queenstown, New Zealand, 2010, pp. 1-8.
- [18] D. K. Prasad and M. K. H. Leung, "Methods for ellipse detection from edge maps of real images," in *Machine Vision - Applications and Systems*, F. Solari, M. Chessa, and S. Sabatini, Eds., ed: InTech, 2012, pp. 135-162.
- [19] X. Bai, C. Sun, and F. Zhou, "Splitting touching cells based on concave points and ellipse fitting," *Pattern Recognition*, vol. 42, pp. 2434-2446, 2009.

- [20] D. K. Prasad, "Adaptive traffic signal control system with cloud computing based online learning," in *8th International Conference on Information, Communications, and Signal Processing (ICICS 2011)*, Singapore, 2011.
- [21] G. Heitz, G. Elidan, B. Packer, and D. Koller, "Shape-based object localization for descriptive classification," *International Journal of Computer Vision*, vol. 84, pp. 40-62, 2009.
- [22] D. K. Prasad and M. K. H. Leung, "Error analysis of geometric ellipse detection methods due to quantization," in *Fourth Pacific-Rim Symposium on Image and Video Technology (PSIVT 2010)*, Singapore, 2010, pp. 58 - 63.
- [23] D. K. Prasad, M. K. H. Leung, and C. Quek, "DEB: Definite error bounded tangent estimator for digital curves," *Image and Vision Computing*, 2012(under review).
- [24] D. K. Prasad, R. K. Gupta, and M. K. H. Leung, "An Error Bounded Tangent Estimator for Digitized Elliptic Curves," in *Discrete Geometry for Computer Imagery*. vol. 6607, ed: Springer Berlin / Heidelberg, 2011, pp. 272-283.
- [25] I. M. Anderson and J. C. Bezdek, "Curvature and tangential deflection of discrete arcs: a theory based on the commutator of scatter matrix pairs and its application to vertex detection in planar shape data," *IEEE Transactions on Pattern Analysis and Machine Intelligence*, vol. PAMI-6, pp. 27-40, 1984.
- [26] D. M. Tsai and M. F. Chen, "Curve fitting approach for tangent angle and curvature measurements," *Pattern Recognition*, vol. 27, pp. 699-711, 1994.
- [27] B. Dubuc and S. W. Zucker, "Complexity, confusion, and perceptual grouping. Part I: The curve-like representation," *Journal of Mathematical Imaging and Vision*, vol. 15, pp. 55-82, 2001.
- [28] D. K. Prasad, C. Quek, and M. K. Leung, "A precise ellipse fitting method for noisy data," in *Image Analysis and Recognition*, A. Campilho and M. Kamel, Eds., ed Aveiro, Portugal: Springer Berlin Heidelberg, 2012, pp. 253-260.
- [29] D. Chaudhuri, "A simple least squares method for fitting of ellipses and circles depends on border points of a two-tone image and their 3-D extensions," *Pattern Recognition Letters*, vol. 31, pp. 818-829, Jul 2010.
- [30] M. Harker, P. O'Leary, and P. Zsombor-Murray, "Direct type-specific conic fitting and eigenvalue bias correction," *Image and Vision Computing*, vol. 26, pp. 372-381, 2008.
- [31] E. S. Maini, "Enhanced direct least square fitting of ellipses," *International Journal of Pattern Recognition and Artificial Intelligence*, vol. 20, pp. 939-953, 2006.